

# PCCP

Accepted Manuscript



This is an *Accepted Manuscript*, which has been through the Royal Society of Chemistry peer review process and has been accepted for publication.

*Accepted Manuscripts* are published online shortly after acceptance, before technical editing, formatting and proof reading. Using this free service, authors can make their results available to the community, in citable form, before we publish the edited article. We will replace this *Accepted Manuscript* with the edited and formatted *Advance Article* as soon as it is available.

You can find more information about *Accepted Manuscripts* in the [Information for Authors](#).

Please note that technical editing may introduce minor changes to the text and/or graphics, which may alter content. The journal's standard [Terms & Conditions](#) and the [Ethical guidelines](#) still apply. In no event shall the Royal Society of Chemistry be held responsible for any errors or omissions in this *Accepted Manuscript* or any consequences arising from the use of any information it contains.

**Carbon dioxide interaction with isolated imidazole or attached on gold clusters and surface: competition between  $\sigma$  H-bond and  $\pi$  stacking interaction**

Muthuramalingam Prakash <sup>a)</sup>, Kévin Mathivon <sup>a)</sup>, David M. Benoit <sup>b)</sup>, Gilberte Chambaud <sup>a)</sup> and Majdi Hochlaf <sup>a)</sup> \*

a) Université Paris-Est, Laboratoire Modélisation et Simulation Multi Echelle, MSME UMR 8208 CNRS, 5 bd Descartes, 77454 Marne-la-Vallée, France

b) University of Hull, Department of Chemistry, Cottingham Road, Hull, HU6 7RX, UK.

---

\* Corresponding author: M. Hochlaf: phone: +33 1 60 95 73 19. FAX: +33 1 60 95 73 20. Email:

[hochlaf@univ-mlv.fr](mailto:hochlaf@univ-mlv.fr)

**Abstract**

Using first principle methodologies, we investigate the subtle competition between  $\sigma$  H-bond and  $\pi$  stacking interaction between CO<sub>2</sub> and imidazole either isolated, adsorbed on a gold cluster or adsorbed on a gold surface. These computations are performed using MP2 as well as dispersion corrected density functional theory (DFT) techniques. Our results show that the CO<sub>2</sub> interaction goes from  $\pi$ -type stacking into  $\sigma$ -type when CO<sub>2</sub> interacts with isolated imidazole and Au clusters or surface. The balance between both types of interactions is found when an imidazole is attached to a Au<sub>20</sub> gold cluster. Thus, the present study has great significance in understanding and controlling the structures of weakly-bound molecular systems and materials, where hydrogen bonding and van der Waals interactions are competing. The applications are in the fields of the control of CO<sub>2</sub> capture and scattering, catalysis and bio- and nanotechnologies.

## I. Introduction

Charge transfers through covalent and noncovalent interactions are playing a vital role in biomolecular devices and material applications.<sup>1,2</sup> For instance, functionalization of materials for CO<sub>2</sub> capture is currently an active area of research in chemical and environmental sciences<sup>3</sup> through the development of nanodevices that are reducing environmental pollutant concentration in the atmosphere. One of the most promising material developments for carbon capture and sequestration (CCS) is storage as solid adsorbents through chemisorption.<sup>4</sup> Even though amine based materials are good adsorbents, these methods have certain drawbacks.<sup>5</sup> Alternatively, adsorption through physisorption is used. The adsorption or desorption of gases through this process requires relatively less energy when compared to the former one. Adsorption on coinage metals (such as Cu, Ag, and Au) is viewed as a promising route for materials for future technologies and applications as pointed out in Refs.<sup>6,7,8,9</sup>

Interaction of small molecule(s) such as CO<sub>2</sub>,<sup>10</sup> CO,<sup>11</sup> NO<sub>2</sub>,<sup>12</sup> NH<sub>3</sub>,<sup>13</sup> H<sub>2</sub>O,<sup>14,15</sup> H<sub>2</sub>S<sup>16</sup> and thiols<sup>17</sup> on Au(111) surface received widespread attention. Particularly, the experimental studies by Farkas and Solymosi showed that the interaction between CO<sub>2</sub> and a gold surface is very weak, whereas radical formation with potassium enhances the adsorption of CO<sub>2</sub> on Au(111) surface.<sup>10</sup> The capture of CO<sub>2</sub> can be enhanced by functionalizing gold clusters, surfaces or self-assembled monolayers (SAMs). Previous investigations used nitrogen-based biomolecules such as guanine (G),<sup>18,19</sup> cytosine (C),<sup>20,21</sup> adenine (A),<sup>22</sup> thymine (T),<sup>23</sup> uracil (U),<sup>24</sup> histidine<sup>25</sup>, cysteamine<sup>26</sup> and DNA base pairs (AT and GC)<sup>27,28,29,30,31</sup> with gold clusters and surfaces. At the microscopic level, the mechanisms of such enhancement are still unknown and worth investigating with modern computational chemistry.

In the present contribution, we have used *ab initio*, both wave-function and DFT methodologies, to investigate the interaction between CO<sub>2</sub> and imidazole (*Im*) either isolated, attached to a gold cluster or to a gold surface. *Im* and *Im* derivatives are the main organic molecular linker in the Zeolitic Imidazolate Frameworks (ZIFs), a subclass of Metal-Organic Frameworks (MOFs) that are promising materials for CO<sub>2</sub> adsorption and gas separation.<sup>32,33,34</sup> Our choice of *Im* – gold system is also motivated by the recently reported role and characterization of gold-imidazole nanoparticles in chemical and biological sensing<sup>35</sup> and *in vivo* and *in vitro* targeted drug delivery.<sup>36</sup> *Im* is also used as corrosion inhibitor and possible adhesion promoter for electric devices.<sup>37</sup>

## II. Computational Details

The geometries of the *Im*@Au<sub>20</sub> clusters and of the CO<sub>2</sub>-*Im* and the CO<sub>2</sub>-*Im*@Au<sub>20</sub> complexes were fully optimized using density functional theory along with the Perdew–Burke–Ernzerhof (PBE) GGA exchange–correlation functional<sup>38</sup> as implemented in Gaussian 09.<sup>39</sup> For gold, we used Los Alamos effective relativistic core potential (ECP) Lanl2DZ and the associated 6-31+G\*\*ULanl2DZ basis set.<sup>40</sup> The H, C, O and N atoms were described using the aug-cc-pVTZ

Dunning and co-workers' basis set.<sup>41,42</sup> Further computations were performed at the Møller–Plesset second-order perturbation (MP2) theory<sup>43</sup> and with Truhlar's hybrid meta-GGA functional (i.e. M05-2X).<sup>44</sup>

Gold surface calculations were carried out with the Quickstep<sup>45</sup> module of the CP2K program package version 2.2<sup>46</sup> using DFT-PBE. The CP2K package adopts a hybrid basis set formalism known as a Gaussian and Plane Wave<sup>47</sup> (GPW) method where the Kohn–Sham orbitals are expanded in terms of contracted Gaussian type orbitals (GTO), while an auxiliary plane wave basis set is used to expand the electronic charge density. In this study, atomic structures of gold Au(111) surface are taken from previously resolved global minimum structures on the basis of combined photoelectron spectroscopy (PES) measurements.<sup>48</sup> We use a slab approach to simulate the Au(111) surface which consists of three layers of 48 gold atoms each. Only the bottom layer was fixed and the two upper layers were fully optimized throughout the study. The unit cell parameters were  $a = 20.93 \text{ \AA}$ ,  $b = 12.54 \text{ \AA}$ ,  $c = 10.70 \text{ \AA}$ ,  $\alpha = 90^\circ$ ,  $\beta = 90^\circ$  and  $\gamma = 90^\circ$ . The calculations were performed at the gamma-point of the Brillouin zone. Valence electrons were treated explicitly, whereas core electrons were described using norm-conserving Goedecker–Teter–Hutter (GTH) pseudopotentials.<sup>49</sup> The molecularly optimized triple-zeta valence basis set with one polarization function (TZV2P-MOLOPT-GTH) was used for all atoms except gold, for which the shorter range molecularly optimized double-zeta basis set with one polarization function (DZVP-MOLOPT-SR-GTH) was used.<sup>50</sup> Both 5d and 6s electrons of Au were included in the valence and we used an auxiliary plane wave cut-off of 400 Ry.

To address long range interactions, such as hydrogen bonding (H-bonding) and van der Waals interactions (vdWs), we used Grimme's latest version of empirical correction term (DFT-D3).<sup>51,52,53</sup> We performed single-point energy correction for the geometries optimized using PBE.

### III. Results

The binding energies (BEs) were calculated using the following energy expression:

$$BE = (E_{AB} - (E_A + E_B)) \quad (1)$$

For  $\text{CO}_2\text{-}Im$  and  $\text{CO}_2\text{-}Im@Au_{20}$  complexes, the computations were performed within the supermolecule approach and corrected for basis set superposition error (BSSE) using the procedure suggested by Boys and Bernardi.<sup>54</sup> Here,  $E_{AB}$  is the total energy of the complex at equilibrium,  $E_A$  is the energy of the monomer  $Im$  or  $Im@Au_{20}$  and  $E_B$  is the energy of  $\text{CO}_2$ , where the energies of the complex and the monomers were computed in the full basis set of the complex. For  $\text{CO}_2\text{-}Im@Au(111)$  and  $Im@Au(111)$ ,  $E_{AB}$  correspond to their total energies at equilibrium,  $E_A$  are those of  $\text{CO}_2$  or  $Im$  and  $E_B$  is the energy of  $Im@Au(111)$  or  $Au(111)$ , respectively. Using expression (1), BEs have negative values for stable complexes, where the monomers were kept fixed to their optimized equilibrium geometries before complexation.

The main geometrical parameters and the corresponding binding energies are listed in Table 1 and Figures 1 - 3. These BEs are computed with and without considering the D3 dispersion for comparison.

#### a. $\text{CO}_2 - \text{Im}$

Three isomeric forms were found for the  $\text{CO}_2 - \text{Im}$  complex. They are displayed in Figure 1. However, only those denoted by Model I and Model II (Table 1 and Figure 1) are relevant for the present study since third conformation (referred as MIN) doesn't allow for possible binding to the Au surface or cluster. In 2009, Froudakis and co-workers<sup>55</sup> investigated the interactions between  $\text{CO}_2$  and N-containing organic heterocycles at the CCSD(T)/CBS level of theory. Similar to the  $\text{CO}_2 - \text{Im}$  complex, in-plane MIN type structures turn out to be the most stable forms. This is due to favorable electron donor-electron acceptor (EDA) mechanism between the carbon of  $\text{CO}_2$  and the nitrogen of the heterocycle and to weak hydrogen bonds. All of them stabilize hence such complexes. In the following, MIN structure will not be considered since the lone pair of nitrogen binding to  $\text{CO}_2$  cannot undergo another bonding with Au. This clearly reveals that MIN mode of interaction is not favorable at Au surface. The calculated distances ( $\text{N1}\cdots\text{C}$  and  $\text{C-H}\cdots\text{O}$  ( $\sim 2.7$  Å)) and geometry of the complex shows that quadrupole and induced dipole interactions are in action. Indeed, considerable charge separation in  $\text{C}=\text{O}$  bond results on a relatively large quadrupole moment.

The bonding in Model I isomer is ensured by a  $\sigma$  type H-bond ( $\text{N-H}\cdots\text{O}$ ) whereas a  $\pi$  type stacking interaction is responsible for bonding in Model II form. The intermonomer distances are evaluated 2.2 Å and of 3.1 Å for Model I and Model II, respectively. These distances are consistent with the bonding type of each complex as well documented by Froudakis and co-workers.<sup>55</sup>

At the PBE-D3/aug-cc-pVTZ level, we compute BEs of  $-9.3$  and  $-11.1$  kJ/mol for Model I and Model II, respectively. The use of M05-2X functional or MP2 is in favor for the stabilization of Model II isomer. For instance, Model I M05-2X-D3/aug-cc-pVTZ BE is calculated  $-9.1$  kJ/mol i.e. about 2/3 of Model II M05-2X-D3/aug-cc-pVTZ BE (of  $-15.1$  kJ/mol). Such behavior is not surprising and was recently reported in the benchmark studies of the  $\pi-\pi$  interactions between  $\text{CO}_2$  and benzene, pyridine, and pyrrole by Chen et al.<sup>56</sup> At the MP2/aug-cc-pVTZ level, we compute a  $\pi$  stacking  $\text{CO}_2 - \text{Im}$  BE of  $-14.8$  kJ/mol, which is consistent with that computed by Chen et al. at the same level of theory for T-pyrrole -  $\text{CO}_2$  complex (of  $-15.4$  kJ/mol). Our work shows however the importance of the inclusion of Grimme's dispersion term for an accurate description of the long range type interactions (H-bonding and vdWs interaction) since this term contributes up to 15–50% to BE of Model II. Nevertheless,  $\sigma$  type H-bond ( $\text{N-H}\cdots\text{O}$ ) seems to be less sensitive to this term.

#### b. $\text{Im}@Au_{20}$ and $\text{CO}_2 - \text{Im}@Au_{20}$

Detailed benchmark studies on gold nanoclusters ( $\text{Au}_n$ ; where  $n=2 - 20$ ) with  $\text{Im}$  have shown that reactivity and stability depends on the size of the gold nanoclusters (unpublished results).<sup>57</sup> Presently, we choose  $\text{Au}_{20}$  cluster of highly symmetrical tetrahedral ( $T_d$ ) geometry, which mimics the bulk phase fcc gold surface. Figure 2 displays the optimized structures for  $\text{Im}@Au_{20}$  and for  $\text{CO}_2 -$

*Im*@Au<sub>20</sub>. This figure shows that the highly symmetric T<sub>d</sub> structure is slightly perturbed by attaching *Im*. The Au atom attached to *Im* is now promoted out of the surface of the Au<sub>20</sub> cluster. The calculated BEs for (*Im*@Au<sub>20</sub>) using PBE and M05-2X with aug-cc-pVTZ basis set are -34.0 and -53.0 kJ/mol, respectively. *A priori*, M05-2X functional overestimates the BEs of surface model. Nevertheless, Prakash et al. showed that this functional may lead to reliable description of noncovalent interactions<sup>58</sup>, close to CCSD(T)/CBS limit<sup>59</sup>). The inclusion of D3 correction increases the PBE BE by ~30 kJ/mol to -63.7 kJ/mol (see Table 1).

For *Im*@Au<sub>20</sub>, we identified three bonds between *Im* and the Au cluster surface:

(i) a strong interaction between the nitrogen (N1) of *Im* and Au evidenced by a relatively short N-Au distance (of ~2.4 Å), which is the signature of the occurrence of a covalent bond. The electron density isosurface (cf. supplementary material, Figure S1) shows that the bonding between N and Au is due to a charge transfer between Au and N1, resulting in a covalent heteroatom-metal interaction.<sup>57</sup> Recent theoretical studies on guanine with gold nanoparticles are in line of these findings.<sup>19</sup> The fragmented orbital analysis reveals that there is electron donation from the N lone pair to the unoccupied orbital of the Au<sub>n</sub> clusters. In addition,  $\pi$  back donation also from the polarized d<sub>yz</sub> orbital (Au) to the p<sub>y</sub>- $\pi^*$  (N) orbital takes place. For further details, readers are referred to our benchmark studies on *Im*@Au<sub>n</sub> clusters.<sup>57</sup>

(ii) two weak type H-bondings (C-H...Au) with a H...Au distance of ~3 Å. These additional unconventional H-bonds stabilize this complex. These three *Im*-Au interactions are of  $\sigma$  type. They are preferable to the possible  $\pi$  stacking of *Im* to Au, which leads to less stable isomeric forms (not shown here). This results into an *Im* perpendicular to the Au surface of the Au<sub>20</sub> cluster, which preserves the T<sub>d</sub> symmetry. These findings are detailed in our recent benchmark studies on *Im* interacting with gold clusters.<sup>57</sup>

For CO<sub>2</sub> - *Im*@Au<sub>20</sub>, two isomeric forms were found: Type Model I with a N-H...O, H-bond and Type Model II where *Im* and CO<sub>2</sub> are stacked (Figure 2). For Model I, we compute N1-Au and N-H...O distances of ~ 2.4 Å and 2.1 Å respectively. For CO<sub>2</sub> - *Im*@Au<sub>20</sub> Model II, N1-Au is slightly shorter than in CO<sub>2</sub> - *Im*@Au<sub>20</sub> Model I. The distances between CO<sub>2</sub> and the adsorbed *Im* on Au<sub>20</sub> are of ~3.8/3.4 Å, which are distinctly longer than between CO<sub>2</sub> and the isolated *Im* (Table 1). The lengthening of the CO<sub>2</sub> - *Im* distance upon adsorption is due to the weakening of the  $\pi$  stacking type bonding between CO<sub>2</sub> and *Im* in CO<sub>2</sub>- *Im* @Au<sub>20</sub>. This is related to the strong perturbations of the electron density of the *Im* ring upon complexation and the creation of the Au-N bond as noticed above. This is also illustrated in Figure S2 of the supplementary material. This figure reveals that charge transfer through an H-bonded model is more favorable than the  $\pi$  stacking of CO<sub>2</sub> on *Im* functionalized gold clusters.

At the PBE/aug-cc-pVTZ level of theory, we compute BEs of -10.5 and -6.3 kJ/mol in favor of Model I. After inclusion of D3 corrections, BEs of Model I and Model II are close (~ -12 kJ/mol).

Therefore, the contribution of D3 corrections ( $\Delta E$ ) for Model I and Model II are  $-1.3$  and  $-5.6$  kJ/mol, respectively (Table 1). This clearly reveals that Model II complex is mostly stabilized through long range dispersion interaction whereas Model I contains strong N-H $\cdots$ O H-bonding. One can note that these BEs are compatible with the calculated distances between the complexes. Again, M05-2X slightly overestimates the BEs compared to their corresponding values computed with PBE.

**c. *Im*@Au(111) and CO<sub>2</sub> - *Im*@Au(111)**

The interaction of an adsorbate (*Im* here) with the Au(111) surface may occur at three distinct positions: namely top (t); bridge (b) and hcp-hollow (h) (Figure 3). The optimized geometries of *Im*@Au(111) and of CO<sub>2</sub> - *Im*@Au(111) are shown in Figure 3 along with the main geometrical parameters. The respective geometrical distances and BEs are presented in Table 1.

The surface calculations started with constrained bottom layer at PBE/DZVP (for Au SZV) followed by PBE/TZVP (for Au DZVP). It can be found from our periodic boundary condition (PBC) computations, that the most favorable mode of interaction at gold surface is a *top* site with unprotonated N1 atom of *Im*. After optimization at PBE/TZVP, the top site interaction of *Im* Au $\cdots$ N distance is  $2.376$  Å with exactly perpendicular *Im* to the surface (the angle between the gold surface and *Im* plane is  $\sim 90^\circ$ ). This agrees with the recent combined soft X-ray photoelectron (XPS) and near edge X-ray absorption fine structure (NEXAFS) spectroscopic investigations of cyclo(glycyl-histidyl) and cyclo(phenylalanyl-prolyl) on Au(111)<sup>60</sup>, and the spectroelectrochemical studies of the electrosorption of imidazole on a gold electrode by Holze.<sup>61</sup> Both works indicated a molecular adsorption to gold surface with a perpendicular orientation. The other favorable positions of *Im*@Au(111) surfaces are bridge and hollow sites. DFT-PBE PBC calculations have shown that bridge site *Im* conformation slightly differs from top site *Im* position. Indeed, *Im*@Au(111)(bridge) plane is not exactly perpendicular to the surface. Instead, it is slightly tilted towards the surface. The calculated Au $\cdots$ N distance and angle are  $2.360$  Å and  $\sim 88^\circ$ , respectively. Furthermore, a tilted conformation has been observed for the hollow site interaction with Au $\cdots$ N distance and tilted/inclined angle (of  $\sim 86^\circ$ ). The calculated distance between Au and N1 atoms is about  $\sim 2.4$  Å which is closer to the pure covalent ( $2.18$  Å) bond rather than to the vdW ( $3.21$  Å) contact distance of Au and N atoms. This is confirmed by our surface PBC calculation (cf. Figure S2 of the supplementary material), which clearly reveals that *Im* forms covalent bond with the Au(111) surface. Consequently, these small changes in geometrical parameters (from perpendicular to inclined) induce large differences in BEs due to the favorable orbital overlap between Au and N1 atom (lone pair) at top site and the less favorable overlap for the other positions. The calculated PBE/TZVP BEs of top, bridge and hollow conformation are  $-42.1$ ,  $-23.4$ , and  $-20.7$  kJ/mol, respectively. The first value is consistent with the earlier DFT-PBE value reported for histidine@Au(111) (of  $-45.6$  kJ/mol) adsorbed on top position.<sup>25</sup>

In order to quantify the role of dispersive and vdW interactions between surface and substrate, we incorporated DFT-D3 term, which leads to a significant enhancement in the BEs because of the

crucial role played by the dispersive terms in the stability of these complexes. The calculated BEs at PBE with DFT-D3 level in bridge, top, and hollow are  $-69.4$ ,  $-67.5$ , and  $-67.5$  kJ/mol, respectively. Note that adsorptions at the top and hollow sites become degenerate for this level of theory. Moreover tilted conformations ( $Im@Au_b$  and  $Im@Au_h$ ) have larger  $\Delta E$  effects than the  $Im@Au_t$  site interactions (Table 1). Recent reports on the DNA base pairs in interaction with gold surface have shown that vdW interactions play crucial role in the geometries and energetics of the complexes.<sup>62</sup> This is in line with our findings.

Figure 3 displays the  $CO_2 - Im@Au(111)$  optimized geometries. Again, two configurations are found: (i) where the  $CO_2$  is bound to  $Im$  by an H-bond (Model I) and (ii)  $CO_2$  interacts to the chemisorbed  $Im$  by  $\pi$  stacking type interaction (Model II). In Model I configuration,  $Im$  remains perpendicular to the Au surface whereas  $Im$  is inclined by  $\sim 25^\circ$  to the Au(111) surface in Model II (Table 1). This induces strong perturbations on the overlap between the orbitals of  $Im$  and of Au. This results in a positive BE for Model II without inclusion of dispersion D3 term. After inclusion of this term, Model II is predicted to be bound with a small BE (of  $\sim -4.5$  kJ/mol). In contrast, a large BE is evaluated for Model I with or without D3 (of  $\sim -20$  kJ/mol). This corresponds to a reversed situation with respect to the isolated  $CO_2 - Im$  complex described earlier.

#### IV. Discussion

Our study shows that interaction of  $CO_2$  with  $Im$  is occurring either via  $\sigma$  H-bond or  $\pi$  stacking interactions. In gas phase,  $CO_2$  adsorption at Model II ( $\pi$  stacking) is more stable than Model I ( $\sigma$  H-bond). For an  $Im@Au_{20}$ , both interactions are of similar strength leading to comparable BEs. Whereas a reversed situation, in favor of H-bond is found when  $CO_2$  bonds to an  $Im$  attached to a gold surface. This modulation of weak interaction upon complexation is worth exploring. This represents an important phenomenon for gas storage processes on monolayers of  $Im$  at gold surface or clusters. Indeed, we show for the first time that the competition between  $\sigma$  H-bond and  $\pi$  stacking interaction between  $CO_2$  and  $Im$  may be modulated after attaching the  $Im$  to a gold cluster or a gold surface. On a related topic, Das and coworkers recently reported about competition between H-bonding and dispersion as well as conventional H-bonding with  $\pi$  models using combined experimental and theoretical methods.<sup>63,64</sup> They also scrutinized the competition between a weak  $n \rightarrow \pi^*_{Ar}$  and a strong H-bond (N-H $\cdots$ N) interaction present in the complexes of 7-azaindole with a series of 2, 6-substituted fluoropyridines.<sup>65</sup> These authors showed how the weak interaction modulates the overall structural motif of these complexes in the presence of the strong interaction.

This effect was also observed in solution. Indeed, Zhang et al.<sup>66</sup> used DFT and  $^{13}C$ -NMR approaches to point out the existence of competition between  $\pi \cdots \pi$  interaction and halogen bond in the binary liquid mixtures of  $C_6D_6$  with  $C_6F_5X$  ( $X = Cl, Br, I$ ). For  $X = Cl, Br$ , their experimental and theoretical results clearly show that there are no  $C-X \cdots \pi$  halogen bonds and that only the  $\pi \cdots \pi$  interactions exist. In contrast, both  $C-I \cdots \pi$  halogen bonds and  $\pi \cdots \pi$  interactions are present in the

binary liquid mixtures of  $C_6D_6$  with  $C_6F_5I$ . As stated there, the entropy is dominating the competition between  $\pi\cdots\pi$  interaction and halogen bond in solution.

Therefore, the competition between weak interactions may occur at substrate – solid surface interfaces and not only in gas phase or in solution. The control of the bonding between the substrate – solid surface entities opens the way for a wide range of applications. For instance, we can cite the fields where gold plays an important role such as in sensors, biosensors, drug-delivery, molecular electronic devices and energetic materials<sup>67,68</sup> and for the design of new materials for  $CO_2$  capture and sequestration.

In addition, this work establishes *Im* as viable anchor for gold surfaces. This N-heterocyclic organic anchor has a relatively low BE, which is  $\sim 1/4$  of that of N-heterocyclic carbene (ANHC) anchors on gold surfaces<sup>69</sup> and  $\sim 1/3$  of that of the S–Au bond in thiols chemisorbed on gold surfaces S–Au monolayers.<sup>70</sup> New applications are expected since this low BE can lead to monolayer desorption at moderate and ambient temperatures (less than  $100^\circ C$ ).

## V. Conclusion

The interaction of  $CO_2$  with three categories (i.e. isolated *Im*, *Im* attached to a gold cluster and *Im* attached to a gold surface) is investigated using *ab initio* (DFT) approaches. We show that the inclusion of dispersive terms is crucial for the correct description of this kind of systems. Adsorption of molecules at gold surface mainly depends on the vdWs interaction and dispersion character. For instance, the prediction of exact binding sites of atoms and molecules on metal surface is not straightforward. Moreover, we show that the strength of the interaction between adsorbate and metal surface depends clearly on the quality of functional and on the inclusion of dispersion correction. Additionally, our results show that the equilibrium structures result on the competition between two types of weak interactions between  $CO_2$  and *Im*: either H-bond or  $\pi$  stacking. The origins of such behavior are detailed.

From an application point of view, it can be concluded that a gold surface enhances the *Im* capacity to adsorb  $CO_2$  through charge transfer process and electrostatic H-bonded interaction in [N–H $\cdots$ O( $CO_2$ )] Model-I, whereas the  $\pi$  stacked Model-II  $CO_2$  adsorption capacity is decreased. This is due to the substantial charge transfer from one side of the aromatic  $\pi$ -cloud of *Im* moiety to the gold surface. In addition, our stacked model reveals that adsorption/desorption mechanism occurs at particular conformations. This is worth further investigated for gas storage processes on monolayers of *Im* at gold surfaces.

The present findings may be complemented by dynamical simulations similar to the recent work on the electron transfer processes in alkanethiolate self-assembled monolayers at the Au(111) surface.<sup>2</sup> As pointed out presently, this work suggests a rational control of the dynamics of the electron transfer process via the modulation of the interactions between the organic and the gold surface.

**Acknowledgments**

This research was supported by a Marie Curie International Research Staff Exchange Scheme Fellowship within the 7<sup>th</sup> European Community Framework Program under Grant No. PIRSES-GA-2012-31754, the COST Action CM1002 CODECS. M. P. thanks a financial support from the LABEX Modélisation & Expérimentation pour la Construction Durable (MMCD, U. Paris-Est) and fruitful discussions with T. Lelièvre and L. Brochard (ENPC, France). This study was undertaken while M.H. was a Visiting Professor at King Saud University. The support of the Visiting Professor Program at King Saud University is hereby gratefully acknowledged.

**Figure captions**

**Figure 1:** Optimized geometries of CO<sub>2</sub> – *Im* Model-I ( $\sigma$ -type), Model-II ( $\pi$ -type) and MIN, which corresponds to the most stable form. We give also the corresponding BSSE corrected BEs computed at the MP2/aug-cc-pVTZ level.

**Figure 2:** Optimized structures of *Im*@Au<sub>20</sub> and of CO<sub>2</sub> – *Im*@Au<sub>20</sub> complexes.

**Figure 3:** Optimized structures of *Im*@Au(111) and of CO<sub>2</sub> – *Im*@Au(111) complexes at PBE/TZVP method along with the distances (in Å).

**Table 1:** Main geometrical parameters (distances in Å and angles in degrees) and binding energies (BEs, in kJ/mol) of CO<sub>2</sub> - *Im*, *Im*@Au<sub>20</sub>, CO<sub>2</sub> - *Im*@Au<sub>20</sub>, *Im*@Au(111), CO<sub>2</sub> - *Im*@Au(111) computed at the PBE/aug-cc-pVTZ and PBE-D3/aug-cc-pVTZ levels of theory. Further computations for CO<sub>2</sub> - *Im*, *Im*@Au<sub>20</sub>, CO<sub>2</sub> - *Im*@Au<sub>20</sub> are also given See text for more details.

<b>CO<sub>2</sub> - <i>Im</i></b>					
	<b>PBE/aug-cc-pVTZ</b>			<b>PBE-D3/aug-cc-pVTZ</b>	
	<b>N-H...O/N<sub><i>im</i>...C</sub></b>	<b>BE</b>		<b>BE</b>	<b>ΔE<sup>a</sup></b>
CO <sub>2</sub> - <i>Im</i> Model I σ type H-bond (N-H...O)	2.259	-8.0		-9.3	-1.3
	2.221 <sup>b)</sup>	-8.2 <sup>b)</sup>		-9.1	-0.9
	2.133 <sup>c)</sup>	-9.3 <sup>c)</sup>		-	-
CO <sub>2</sub> - <i>Im</i> Model II π Stacking (N <sub><i>im</i>...C</sub> )	-	-5.0		-11.1	-6.1
	3.057 <sup>b)</sup>	-13.8 <sup>b)</sup>		-15.1 <sup>b)</sup>	-1.3 <sup>b)</sup>
	3.082 <sup>c)</sup>	-14.8 <sup>c)</sup>		-	-
<b><i>Im</i>@Au<sub>20</sub></b>					
	<b>PBE/aug-cc-pVTZ</b>			<b>PBE-D3/aug-cc-pVTZ</b>	
	<b>N-Au</b>	<b>C<sub>2</sub>-H...Au</b>	<b>BE</b>	<b>BE</b>	<b>ΔE<sup>a</sup></b>
<i>Im</i> @Au <sub>20</sub>	2.387	3.172	-34.0	-63.7	-29.7
	2.359 <sup>b)</sup>	3.143 <sup>b)</sup>	-53.0 <sup>b)</sup>	-61.3	-8.3
<b>CO<sub>2</sub> - <i>Im</i>@Au<sub>20</sub></b>					
	<b>PBE/aug-cc-pVTZ</b>			<b>PBE-D3/aug-cc-pVTZ</b>	
	<b>N-Au</b>	<b>N-H...O/ N<sub><i>im</i>...C</sub></b>	<b>BE</b>	<b>BE</b>	<b>ΔE<sup>a</sup></b>
CO <sub>2</sub> - <i>Im</i> @Au <sub>20</sub> Model I	2.405	2.139	-10.5	-11.8	-1.3
	2.345 <sup>b)</sup>	2.130 <sup>b)</sup>	-10.7 <sup>b)</sup>	-11.9	-1.2
CO <sub>2</sub> - <i>Im</i> @Au <sub>20</sub> Model II	2.393	3.756	-6.3	-11.9	-5.6
	2.369 <sup>b)</sup>	3.393 <sup>b)</sup>	-9.7 <sup>b)</sup>	-13.6	-3.9
<b><i>Im</i>@Au(111) Surface</b>					
	<b>PBE/TZVP</b>			<b>PBE-D3/ TZVP</b>	
	<b>Au...N</b>	<b>Au-Au-N</b>	<b>BE</b>	<b>Total</b>	<b>ΔE<sup>a</sup></b>
<i>Im</i> @Au (top)	2.376	90	-42.1 -45.6 <sup>d)</sup>	-67.5	-25.4
<i>Im</i> @Au (bridge)	2.360	88	-23.4	-69.4	-46.0
<i>Im</i> @Au (hollow)	2.401	86	-20.7	-67.5	-46.8
<b>CO<sub>2</sub> - <i>Im</i>@Au(111) Surface</b>					
CO <sub>2</sub> - <i>Im</i> @Au(111) Model I	2.361	90	-19.9	-22.6	-2.7
CO <sub>2</sub> - <i>Im</i> @Au(111) Model II	2.449	77	9.7	-4.5	-14.2

- Enhancement of BEs after inclusion of hybrid meta functional for clusters and dispersion term (Grimme correction for surface) at PBE/TZVP calculations [ $\Delta E = ((\text{PBE-D3}) - \text{PBE})$ ].
- This work. M05-2X/aug-cc-pVTZ
- This work. MP2/aug-cc-pVTZ
- Earlier reported value at PBE method is -45.6 kJ/mol from ref. [25] computed at the PBE method.

Figure 1

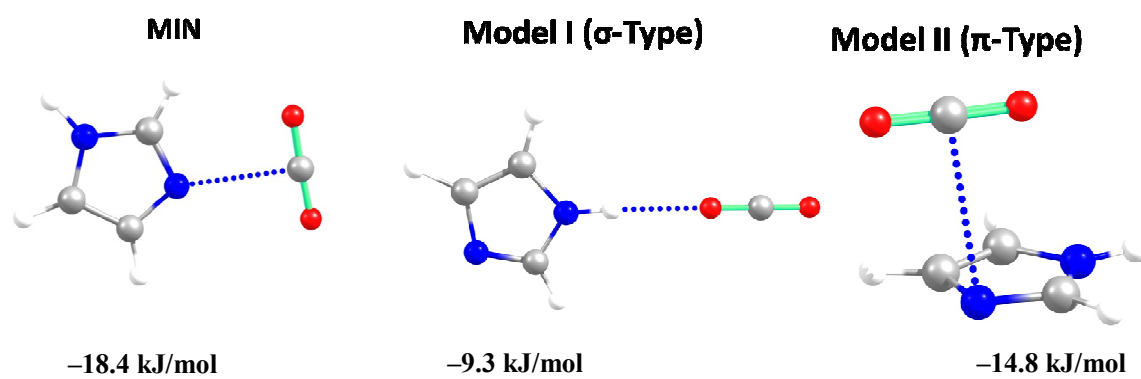


Figure 2

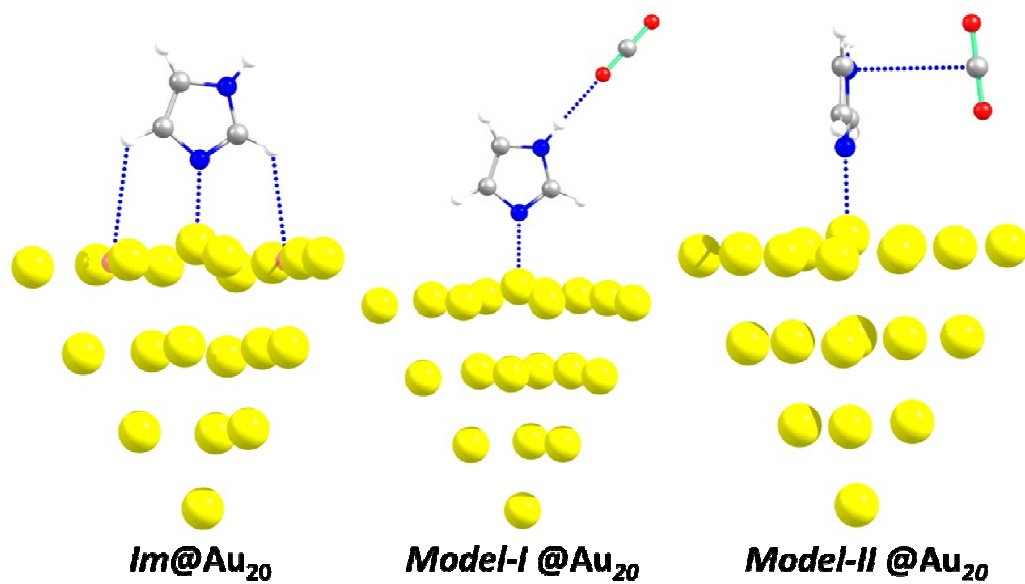
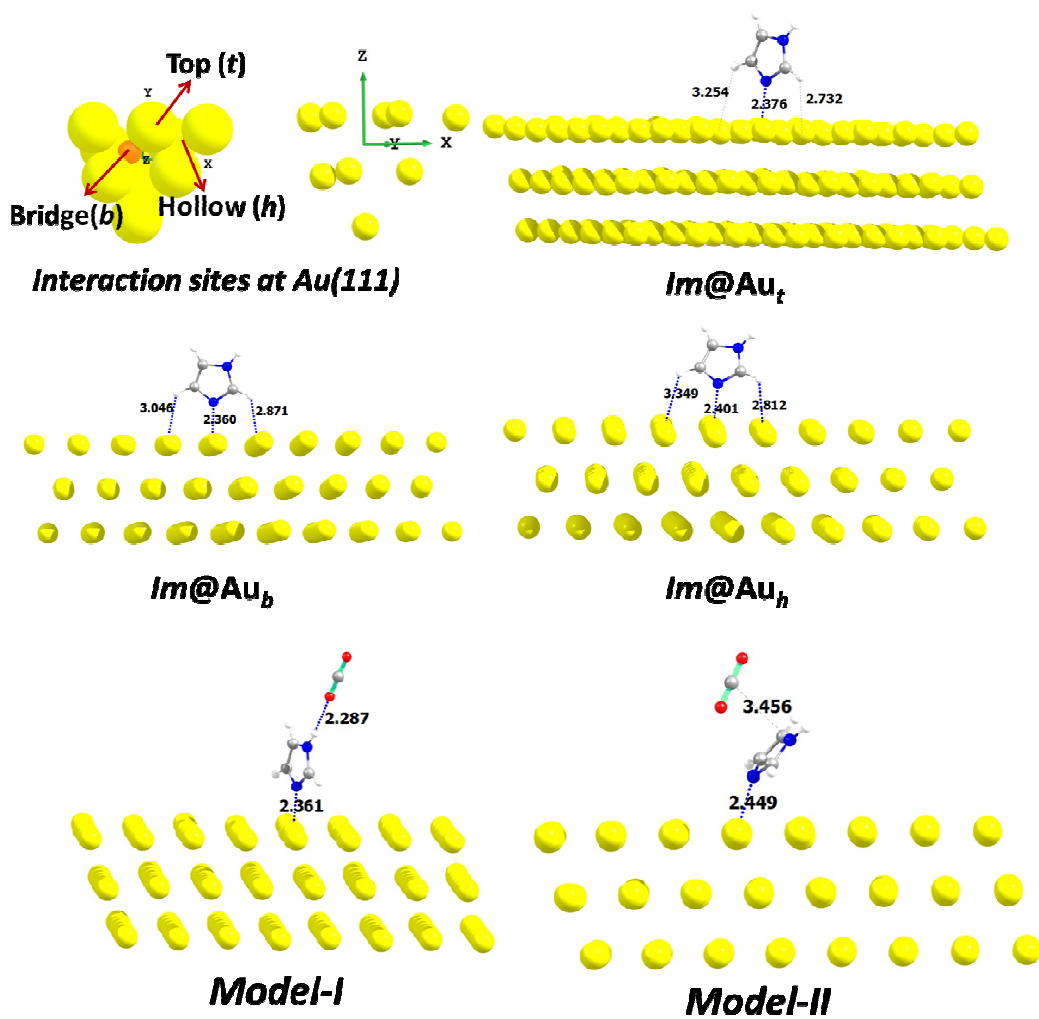
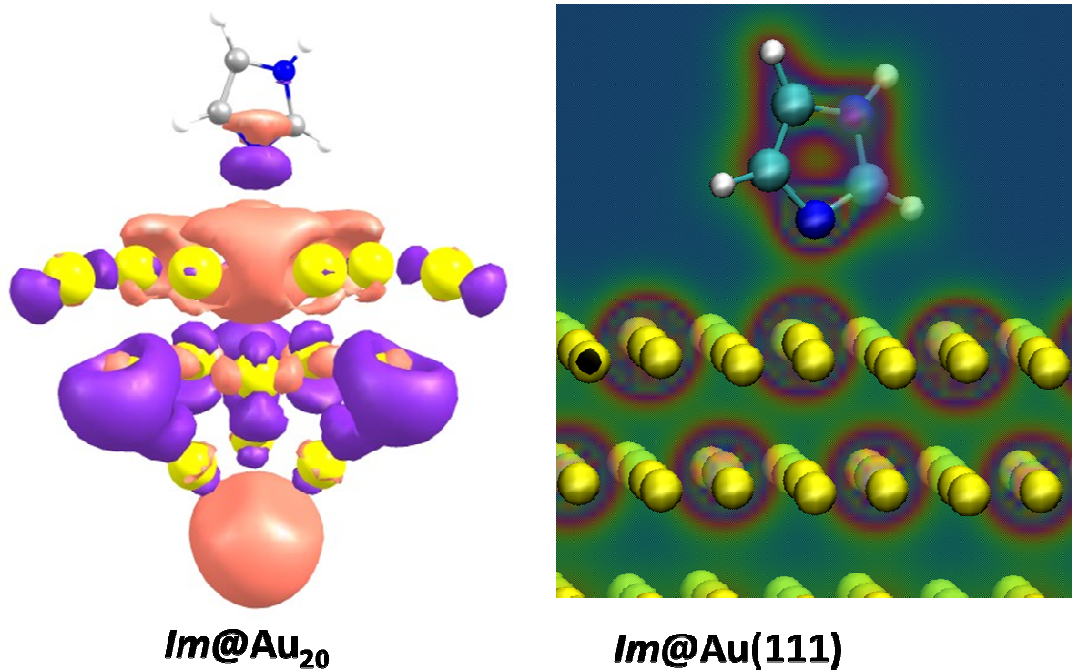


Figure 3

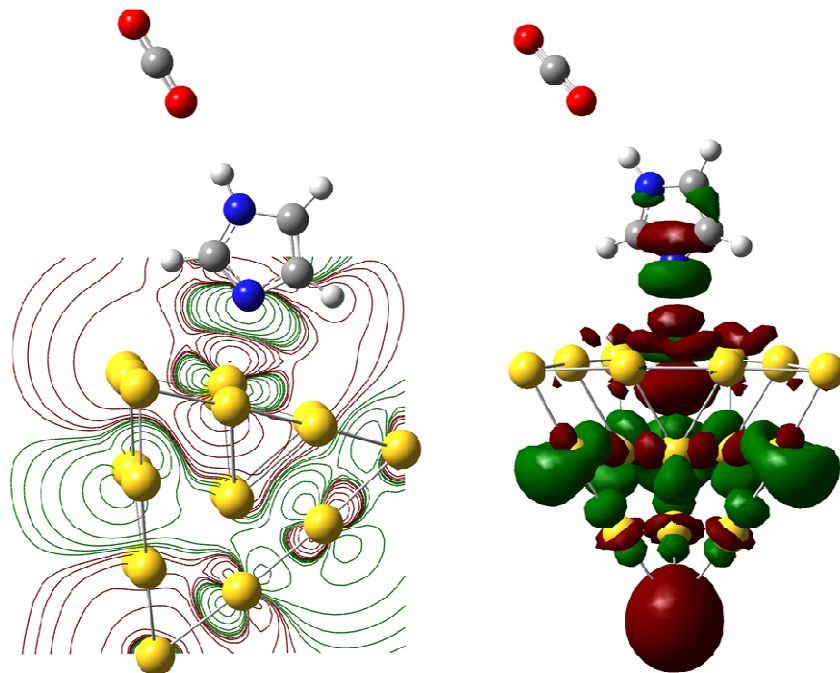


## Supplementary material

**Figure S1:** Electron density surface (isosurface value 0.02 a.u) of  $Im@Au_{20}$  (left) and  $Im@Au(111)$  (right).



**Figure S2:** Iso surface and contour profile for  $\text{CO}_2\text{-Im @Au}_{20}$  (iso surface value 0.02 a.u.).



## References

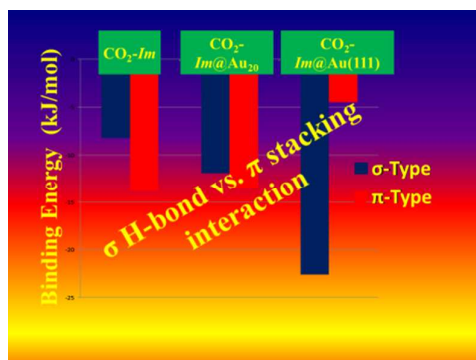
- <sup>1</sup> G. Kladnik, D. Cvetko, A. Batra, M. Dell'Angela, A. Cossaro, M. Kamenetska, L. Venkataraman, and A. Morgante, *J. Phys. Chem. C*, 2013, **117**, 16477–16482.
- <sup>2</sup> V. Prucker, O. Rubio-Pons, M. Bockstedte, H. Wang, P. B. Coto, and M. Thoss, *J. Phys. Chem. C*, 2013, **117**, 25334–25342.
- <sup>3</sup> Y. Liu, J. Liu, M. Chang, and C. Zheng, *J. Phys. Chem. C*, 2012, **116**, 16985–16991.
- <sup>4</sup> J. D. Figueroa, T. Fout, S. Plasynski, H. McIlvried, and R. D. Srivastava, *Int. J. Greenhouse Gas Control*, 2008, **2**, 9–20.
- <sup>5</sup> G. T. Rochelle, *Science* 2009, **325**, 1652–1654.
- <sup>6</sup> K. Tonigold, and A. Gross, *J. Chem. Phys.*, 2010, **132**, 224701.
- <sup>7</sup> S. Grimme, J. Antony, S. Ehrlich, and H. Krieg, *J. Chem. Phys.*, 2010, **132**, 154104.
- <sup>8</sup> W. Liu, V.G. Ruiz, G.-X. Zhang, B. Santra, X. Ren, M. Scheffler, and A. Tkatchenko, *New J. Phys.* 2013, **15**, 053043.
- <sup>9</sup> L. F. Pašteka, T. Rajský, and M. Urban, *J. Phys. Chem. A*, 2013, **117**, 4472–4485.
- <sup>10</sup> A. P. Farkas and F. Solymosi, *J. Phys. Chem. C*, 2009, **113**, 19930–19936.
- <sup>11</sup> T. Zhang, D. A. King, and S. M. Driver, *J. Chem. Phys.*, 2012, **137**, 074703.
- <sup>12</sup> T. Zhang, D. A. King, and S. M. Driver, *J. Phys. Chem. C*, 2012, **116**, 5637–5645.
- <sup>13</sup> E. S. Kryachko, and F. Remacle, *J. Chem. Phys.*, 2007, **127**, 194305.
- <sup>14</sup> G. Cicero, A. Calzolari, S. Corni, and A. Catellani, *J. Phys. Chem. Lett.*, 2011, **2**, 2582–2586.
- <sup>15</sup> R. Nadler and J. F. Sanz, *J. Chem. Phys.*, 2012, **137**, 114709.
- <sup>16</sup> J. Granatier, M. Urban, and A. J. Sadlej, *J. Phys. Chem. A*, 2007, **111**, 13238–13244.
- <sup>17</sup> G. Rajaraman, A. Caneschi, D. Gatteschi, and F. Totti, *Phys. Chem. Chem. Phys.*, 2011, **13**, 3886–3895.
- <sup>18</sup> L. Zhang, T. Ren, X. Yang, L. Zhou, and X. Li, *Int. J. Quantum Chem.*, 2013, **113**, 2234–2242.
- <sup>19</sup> X. Zhang, C. Q. Sun, and H. Hirao, *Phys. Chem. Chem. Phys.*, 2013, **15**, 19284–19292.
- <sup>20</sup> E. S. Kryachko, and F. Remacle, *J. Phys. Chem. B* 2005, **109**, 22746–22757.
- <sup>21</sup> M. Rosa, S. Corni, and R. D. Felice, *J. Phys. Chem. C*, 2012, **116**, 21366–21373.
- <sup>22</sup> A. Kumar, P. C. Mishra, and S. Suhai, *J. Phys. Chem. A*, 2006, **110**, 7719–7727.
- <sup>23</sup> G. Lv, F. Wei, H. Jiang, Y. Zhou, and X. Wang, *J. Mol. Struct. (THEOCHEM)* 2009, **915**, 98–104.
- <sup>24</sup> A. Martinez, *J. Phys. Chem. C*, 2010, **114**, 21240–21246.
- <sup>25</sup> F. Iori, S. Corni, and R. Di Felice, *J. Phys. Chem. C*, 2008, **112**, 13540–13545.
- <sup>26</sup> A. Cossaro, M. Dell'Angela, A. Verdini, M. Puppini, G. Kladnik, M. Coreno, M. Simone, A. Kivimaki, D. Cvetko, M. Canepa, and L. Floreano, *J. Phys. Chem. C*, 2010, **114**, 15011–15014.
- <sup>27</sup> J. J. Storhoff, R. Elghanian, C. A. Mirkin, and R. L. Letsinger, *Langmuir* 2002, **18**, 6666–6670.
- <sup>28</sup> A. Martinez, *J. Phys. Chem. A*, 2009, **113**, 1134–1140.
- <sup>29</sup> M. K. Shukla, M. Dubey, E. Zakar, and J. Leszczynski, *J. Phys. Chem. C*, 2009, **113**, 3960–3966.
- <sup>30</sup> W. Sun, and R. D. Felice, *J. Phys. Chem. C*, 2012, **116**, 24954–24961.
- <sup>31</sup> N. K. Jena, K. R. S. Chandrakumar, and S. K. Ghosh, *J. Phys. Chem. C*, 2012, **116**, 17063–17069.
- <sup>32</sup> R. Banerjee, A. Phan, B. Wang, C. Knobler, H. Furukawa, M. O'Keeffe, and O. M. Yaghi, *Science*, 2008, **319**, 939–943.
- <sup>33</sup> B. Wang, A. P. Cote, H. Furukawa, M. O'Keeffe, and O. M. Yaghi, *Nature*, 2008, **453**, 207–211.
- <sup>34</sup> M. Prakash, N. Sakhavand, and R. Shahsavari, *J. Phys. Chem. C*, 2013, **117**, 24407–24416.
- <sup>35</sup> K. Saha, S. S. Agasti, C. Kim, X. Li, and V. M. Rotello, *Chem. Rev.*, 2012, **112**, 2739–2779.
- <sup>36</sup> G. R. Souza, C. S. Levin, A. Hajitou, R. Pasqualini, W. Arap, and J. H. Miller, *Anal. Chem.*, 2006, **78**, 6232–6237.
- <sup>37</sup> S. Yoshida, and H. Ishida, *J. Chem. Phys.*, 1983, **78**, 6960.
- <sup>38</sup> J. P. Perdew, K. Burke, and M. Ernzerhof, *Phys. Rev. Lett.*, 1996, **77**, 3865–3868.

- 
- <sup>39</sup> M. J. Frisch, *et al.*, *Gaussian 09 (Revision A.02)*, Gaussian, Inc., Wallingford, CT, 2009.
- <sup>40</sup> P. J. Hay, and W. R. Wadt, *J. Chem. Phys.* 1985, **82**, 299–310.
- <sup>41</sup> T. H. Dunning, *J. Chem. Phys.*, 1989, **90**, 1007.
- <sup>42</sup> R. A. Kendall, T. H. Dunning, and R. J. Harrison, *J. Chem. Phys.*, 1992, **96**, 6796.
- <sup>43</sup> C. Møller, and M. S. Plesset, *Phys. Rev.*, 1934, **46**, 618–622.
- <sup>44</sup> Y. Zhao, N. E. Schultz, and D. G. Truhlar, *J. Chem. Theory Comput.*, 2006, **2**, 364–382.
- <sup>45</sup> J. VandeVondele, M. Krack, F. Mohamed, M. Parrinello, T. Chassaing, and J. Hutter, *J. Comput. Phys. Commun.*, 2005, **167**, 103–128.
- <sup>46</sup> C. J. Mundy, F. Mohamed, F. Schiffman, G. Tabacchi, H. Forbert, W. Kuo, J. Hutter, M. Krack, M. Iannuzzi, M. McGrath, M. Guidon, T. D. Kuehne, T. Laino, J. VandeVondele and V. Weber, CP2K software package, <http://cp2k.berlios.de>.
- <sup>47</sup> G. Lippert, J. Hutter, and M. Parrinello, *Theor. Chem. Acc.*, 1999, **103**, 124–140.
- <sup>48</sup> M. T. Nguyen, C. A. Pignedoli, M. Treier, R. Fasel, and D. Passerone, *Phys. Chem. Chem. Phys.*, 2010, **12**, 992–999.
- <sup>49</sup> S. Goedecker, M. Teter, and J. Hutter, *J. Phys. Rev. B* 1996, **54**, 1703–1710.
- <sup>50</sup> J. VandeVondele and J. Hutter, *J. Chem. Phys.*, 2007, **127**, 114105.
- <sup>51</sup> S. Grimme, *J. Comput. Chem.*, 2006, **27**, 1787–1799.
- <sup>52</sup> S. Grimme, *J. Chem. Phys.*, 2006, **124**, 034108.
- <sup>53</sup> S. Grimme, J. Antony, S. Ehrlich, and H. Krieg, *J. Chem. Phys.*, 2010, **132**, 154104.
- <sup>54</sup> S. F. Boys, and F. Bernardi, *Mol. Phys.*, 1970, **19**, 553–566.
- <sup>55</sup> K. D. Vogiatzis, A. Mavrandonakis, W. Klopper, and G. E. Froudakis, *Chem. Phys. Chem.*, 2009, **10**, 374–383.
- <sup>56</sup> L. Chen, F. Cao, and H. Sun, *Int. J. Quantum Chem.*, 2013, **113**, 2261–2266.
- <sup>57</sup> M. Prakash, G. Chambaud, and M. Hochlaf, *J. Chem. Phys.*, (submitted).
- <sup>58</sup> M. Prakash, K. Gopalsamy, and V. Subramanian, *J. Phys. Chem. A*, 2009, **113**, 13845–13852.
- <sup>59</sup> M. Prakash, K. Gopalsamy, and V. Subramanian, *J. Chem. Phys.*, 2011, **135**, 214308.
- <sup>60</sup> O. Plekan, V. Feyer, S. Ptasíńska, N. Tsudd and K. C. Prince, *Phys. Chem. Chem. Phys.*, 2014, **16**, 6657–6665.
- <sup>61</sup> V. R. Holze, *Electrochimica Acta*, 1993, **38**, 947–956.
- <sup>62</sup> M. Rosa, S. Corni, and R. D. Felice, *J. Chem. Theory Comput.*, 2013, **9**, 4552–4561.
- <sup>63</sup> S. Kumar, P. Biswas, I. Kaul, and A. Das, *J. Phys. Chem. A*, 2011, **115**, 7461–7472.
- <sup>64</sup> S. Kumar, V. Pande, and A. Das, *J. Phys. Chem. A*, 2012, **116**, 1368–1374.
- <sup>65</sup> S. K. Singh, S. Kumar, and A. Das, *Phys. Chem. Chem. Phys.*, 2014, **16**, 8819–8827.
- <sup>66</sup> Y. Zhang, B. Ji, A. Tian, and W. Wang, *J. Chem. Phys.*, 2012, **136**, 141101.
- <sup>67</sup> J. Li, X. Li, H. J. Zhai, and L. S. Wang, *Science*, 2003, **299**, 864–867.
- <sup>68</sup> I. Lynch, A. Salvati, and K. A. Dawson, *Nat. Nano*, 2009, **4**, 546–547.
- <sup>69</sup> V. A. Zhukhovitskiy, M. G. Mavros, T. V. Voorhis, and J. A. Johnson, *J. Am. Chem. Soc.*, 2013, **135**, 7418–7421.
- <sup>70</sup> R. G. Nuzzo, B. R. Zegarski, and L. H. Dubois, *J. Am. Chem. Soc.*, 1987, **109**, 733–740.

### Highlights

- Ab initio calculations of imidazole interaction with CO<sub>2</sub>
- Influence of the substrate to which imidazole is adsorbed
- Competition between hydrogen bonding and  $\pi$  stacking interactions

Graphical abstract



Interplay between  $\sigma$  H-bond and  $\pi$  stacking interaction is monitored by the substrate